Weathering in the Glacial Foreland of Southern and Western Greenland

Fabio Da Prat, Ellen Martin

Department of Geological Sciences, University of Florida

Glaciers physically grind up underlying rock and create fine-grained sediment that has a high potential for chemical weathering. Subsequent weathering of these sediments produces solutes, including nutrients and radiogenic isotopes, which are transported by streams to the world's oceans where they can impact primary productivity and record past ice sheet activity. Previous research on the geochemistry of bedrock, bedload sediment and stream waters demonstrated that the extent of chemical weathering varies across a transect in western Greenland due to variations in either exposure age or precipitation (Scribner et al., 2015), and that variations in the extent of weathering associated with retreat of the Greenland Ice Sheet (GrIS) may account for observed trends in solutes during the last deglacial period. This project adds a new study area in southern Greenland that has higher precipitation, more vegetation, a different lithology, and a range of exposure ages, to address the leading factors contributing to the extent of weathering. Based on the relative proportions of cations and percent change between Na+K concentrations of bedload to waters, the southern region is undergoing less extensive weathering than the western transect, which suggests that lithology may be an important driver of weathering, and that exposure age and precipitation are less important factors than expected. The results also suggest there are additional factors that contribute to weathering that were not accounted for in this study, such as dissolved organic matter and microbial activity.

Introduction

As glaciers move over bedrock, they enhance the physical weathering of the rock and produce abundant fine-grained material. The resulting high surface area to volume ratio increases the potential for chemical weathering of the sediment. Chemical weathering in high-latitude, glacial environments could serve as a long-term sink for CO_2 (Anderson et al., 2000) and a source for nutrients and fluxes to the world's oceans (Scribner et al., 2014; Bhatia, et al., 2013). A dramatic increase in seawater Pb isotopes preserved in deep sea sediments from the last deglaciation (~21,000 to 11,000 years ago) has been attributed to intense chemical weathering of freshly exposed, comminuted sediments deposited by the retreating ice sheet (Foster and Vance, 2006). The geochemistry of these sediments, therefore, records the history of ice sheet growth and decay.

The glacial foreland spans from the ice sheet to the continental margin (Fig. 1). Supraglacial water, which originates from melting on top of the ice sheet, and subglacial water, which enters the ice sheet through moulins (vertical shafts in the ice sheet) or melting within the ice and discharges from underneath the ice sheet, combine to form proglacial rivers that carry the meltwater through proglacial watersheds to the ocean. Watersheds that were exposed by ice sheet retreat and are now separated from the ice sheet by hydrologic divides are referred to as deglaciated watersheds. Streams in deglaciated regions originate from active layer melt and local precipitation and are termed non-glacial streams, as their headwaters are not connected to the ice sheet meltwater system.

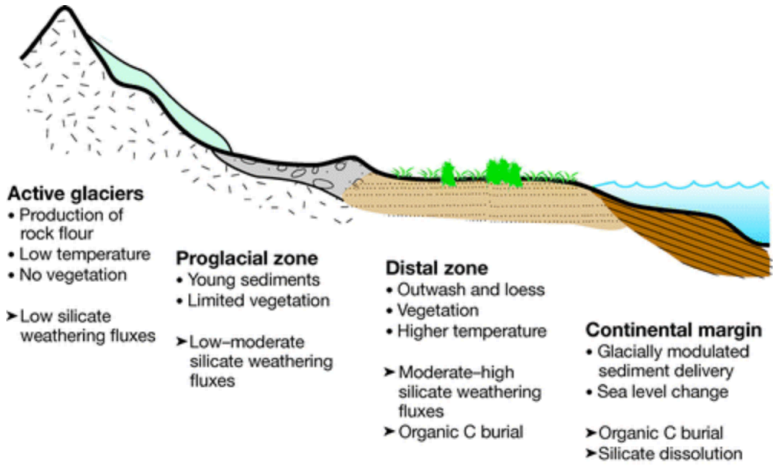

Figure 1. Simplified diagram of zones in the foreglacial environment. Sub- and supraglacial watersheds are associated with the active glacier. These waters feed into proglacial watersheds that transport ice melt to the ocean. Deglaciated watersheds are located in the distal zone that has been exposed by ice sheet retreat, and the associated non-glacial streams are sourced by local precipitation and active layer melt. Figure from Anderson, 2007.

Proglacial rivers have high total suspended solids and low total dissolved solids relative to non-glacial rivers (Wimpenny et al., 2010). These rivers contain a higher proportion of dissolved Ca^{+} and K^{+} ions because of subglacial weathering of trace carbonates and biotite as well as high SO_4^{2-} ions from oxidation of trace sulfates that occurs under the ice sheet (Tranter, 2003; Wimpenny et al., 2010). Studies demonstrate that chemical weathering of glacial sediments preferentially weathers carbonate and sulfate minerals before attacking silicate minerals (Anderson et al., 2000). Analyses of radiogenic isotopes such as Sr and Pb can provide further clues of extent of chemical weathering (Harlavan and Erel, 2002; Blum and Erel, 2003). Preferential weathering of trace minerals, such as biotite, monazite, allanite, and apatite produces weathering solutes with Sr and Pb isotopes that are initially more radiogenic than the bulk rock, but decrease and approach bulk rock values as the extent of weathering increases (Harlavan and Erel, 2002; Blum and Erel, 2003). Solute concentrations in proglacial rivers can increase dramatically as the waters interact with and chemically weather bedload, thus they are sensitive recorders of weathering reactions. In contrast, chemical changes in the bedrock and bedload produced by weathering are masked by high initial concentrations.

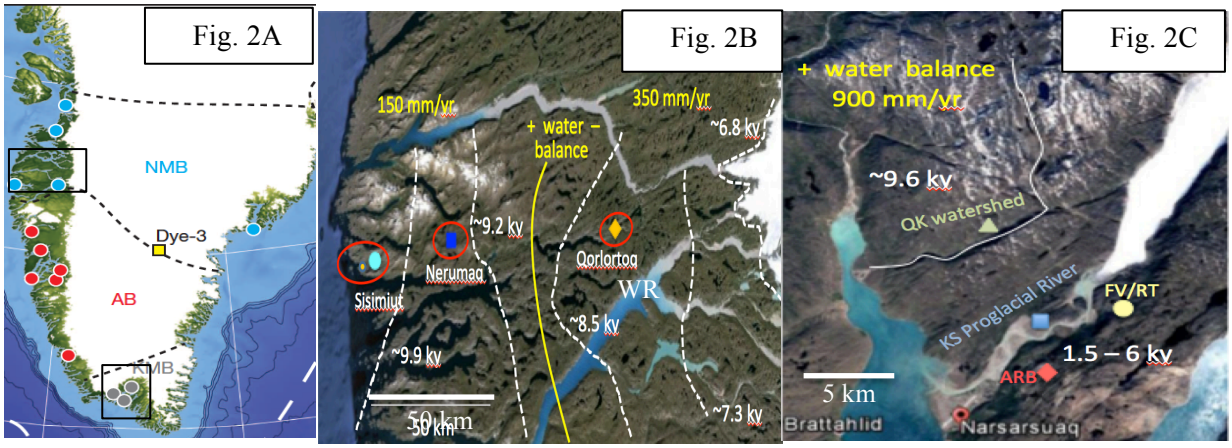

Figure 2. Fig. 2A) Map of Greenland illustrating the major lithological provinces that were analyzed in this study. NBM = Nagsugtiqidian Mobile Belt, AB = Archean Block, KMB = Ketilidian Mobile Belt. Figure modified from Reyes et al., 2014. 2B) Map of western study area showing the locations of Nerumaq, Qorlortoq, and Watson River watersheds that form a transect of increasing weathering maturity from the ice sheet to the coast (Scribner et al., 2015). 2C) Map of southern study area near Narsarsuaq showing location of five sampled watersheds: Qornup Kuua (QK), Flower Valley (FV), Rope trail (RT) and Arboritum (ARB) are deglaciated watersheds. Kiagtut Sermia (KS) is a proglacial river. White text = exposure ages of moraines in each watershed. Yellow text = precipitation information.

Melting of the GrIS over the past 10,000 years exposed a transect of fresh sediments along the margin of western and southern Greenland (Fig. 1 and 2). In the western transect, exposure ages of the deglaciated watersheds increase in age from ~ 7 ka to ~10 ka with increasing distance from the ice (Scribner et al., 2015). There are also Little Ice Age moraines (~200 yrs) adjacent to the GrIS in some areas. The entire western transect is underlain by the Nagsugtiqidian Mobile Belt (NMB) (Fig. 2A) and this lithology remains relatively constant throughout the study region. There is also a precipitation gradient that ranges from 150 mm/year near the ice to 350 mm/year at the coast (Fig. 2B). As a result, the inland vegetation is sparse, mostly composed of tundra and small shrubs. The western Greenland transect thus serves as an exceptional location to understand how exposure age, lithology, and climate affect chemical weathering of sediments in glacial settings.

Scribner et al., (2014) described the differences in weathering across the deglaciated watersheds in the western transect and divided them into 1) coastal deglaciated watersheds that were located in older moraines, exposed to a positive water balance, and exhibited more extensive weathering based on solute concentrations and Sr isotopes, and 2) inland deglaciated watersheds located in younger moraines with a negative water balance and less extensive weathering. Deuerling (2016) used a mass balance model with stream solutes to identify carbonate versus silicate mineral weathering and carbonic acid (H_2CO_3) versus sulfuric acid (H_2SO_4) weathering. She demonstrates that the water compositions reflect a shift from predominantly carbonate weathering inland to predominately silicate weathering near the coast, and that the proportion of weathering by sulfuric acid increases toward the coast (Fig. 3). These changes in weathering are accompanied by a decrease in the offset between dissolved and bedload Sr isotope ratios, and are again interpreted to indicate more mature weathering closer to the coast with increasing exposure age and precipitation. In comparison to the western transect, the southern region has a more variable lithology (Fig. 2A), which includes the Ketilidian Mobile Belt (KMB), and the Gardar Province. The southern region also has higher precipitation (900 mm/year), a warmer climate (~5°C higher, data from the Danish Meteorological Institute), a wide range of exposure ages (~10 to ~1.5 ka) (Fig. 2C), and more vegetation, including trees and larger bushes.

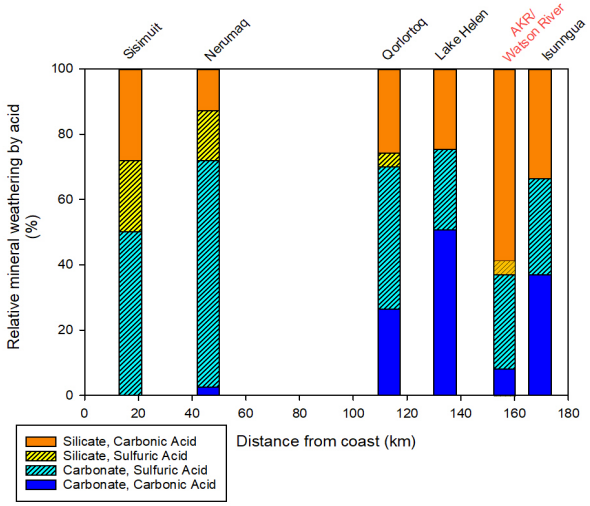

Figure 3. Calculated average relative abundances of chemical weathering divided by mineralogy and acid. Silicate mineral weathering (warm colors) and carbonate mineral weathering (cool colors), carbonic acid (plain pattern) and sulfuric acid (hatched pattern). Names of areas are listed above the bars: black text represents non-glacial streams; red text indicates the proglacial streams draining the entire Watson River watershed. (From Deuerling, 2016)

This study will evaluate the differences in the extent of weathering between the western transect and southern region, as well as within the southern region, by comparing the major element and isotope chemistry of water, bedload, and bedrock. The data for the western transect come from a study by Collazo et al., (2015) that evaluated a coastal deglaciated watershed (Nerumaq), an inland deglaciated watershed (Qorlortoq), and a proglacial system (Watson River; WR). The new data from the southern regions include five deglacial watersheds: Qornup Kuua (QK), Flower Valley (FV), Rope Trail (RT) and Arboritum (ARB), and one proglacial watershed that drains the Kiagtuut Sermia (KS). The bedload samples are believed to represent an integrated composition of bedrock sources in each watershed, and therefore may provide a more accurate record of specific contributions to the watershed. The western water data come from a study by Scribner et al., (2015) and represent a sensitive monitor of weathering reactions. The goal of this study is to compare previous chemical data on bedload, bedrock and dissolved solutes in the water from watersheds in the western transect to the geochemistry in the southern region near Narsarsuaq to understand how precipitation, exposure age, rock type, and vegetation impact chemical weathering of rocks, and ultimately the composition of river runoff transported to the ocean.

Geology of Study Areas

The Nagsugtiqidian Mobile Belt (NMB- 1.7-1.9 Ga) that underlies the western transect is composed of metamorphosed granodiorites and tonalitic orthgneisses of the Archean Belt (AB- 2.6–3.1 Ga). In contrast, the Proterozoic Ketilidian Mobile Belt (KMB- ~1.9-1.7 Ga) that underlies the southern region is composed of granitoids and low- to high-grade metasediments (White et al., 2016). The southern region also contains rocks of the Gardar Province, which is composed of alkaline basalts and sandstones deposited between 1.35-1.12 Ga (Paslick, 1993). This province (Gardar) is interpreted to have been deposited as the result of crustal rifiting that is synchronous to the breakup of paleopangea (Upton et al., 2003).

Methods

Sample Collection

All solid samples were collected in the region of Narsarsuaq, Greenland during August-September of 2017 (Lat: 61.16457°- 61.28543°, Long: 45.31218°- 45.48011°). Bedrock samples were collected from outcrops near the bedload sample sites and were selected to provide a suite of the different lithological units found in the study area. Bedload samples were collected using a plastic trowel or gloved hand and stored in zip-lock bags at each site where waters were sampled.

Water was pumped from the center of river channels through an overflow cup using tygon tubing attached to a Geotech II 12-V peristaltic pump located on river banks. Water was filtered through a 0.45 μm trace metal grade canister filter and collected in sample-appropriate containers after triple rinsing with sample water. Cation (20 ml) samples were collected in acid washed HDPE bottles and acidified in the field to pH < 2 with optima grade nitric acid. All samples were chilled and shipped to the University of Florida within one month of collection.

Sample Preparation

Bedload and bedrock samples were prepared for XRF analyses by crushing, then grinding the samples into a fine powder. Bedload samples were sieved to remove the greater than 2 mm size fraction to avoid any single large grain dominating the analyses. Approximately 1.5 g of fine rock powder underwent loss on ignition (LOI) at about 1000°C for an hour, and LOI was calculated to be, on average, 0.99% of the sample weight. After LOI, one gram (±0.005) of sample was mixed with 6 (±0.005) grams of lithium metaborate flux in order to make glass disks using a Katanax

fusion machine. For isotopic analyses, ~50mg of bedload and bedrock samples were dissolved in concentrated HF:HNO_3 for several days and then dried down. The samples were then converted to nitrates by evaporation with concentrated ultrapure nitric acid. Once dry, the samples were then converted to chlorides by evaporation with ultrapure 6N hydrochloric acid. Once the acid was clear, the samples were dried down one last time and brought up in 1N Seastar HBr before passing through Dowex 1X-8 (100-200 mesh) resin to separate lead for isotope analyses. During the lead elution step the wash was collected for subsequent Sr separation, as the latter is not absorbed on the Dowex resin. The dried residues from the washes were dissolved in 3.5N HNO_3 and loaded on to cation exchange columns packed with strontium-selective crown ether resin (Sr-spec, Eichrom Technologies, Inc.) to separate Sr from other ions following procedure by Pin and Bassin, (1992).

Sample Analysis

The bedload and bedrock samples were analyzed for major elements (SiO_2, TiO_2, Al_2O_3, Fe_2O_3, MnO, MgO, CaO, Na_2O, and K_2O) using a Rigaku "supermini" model wavelength-dispersive x-ray fluorescence. Precision is ±1% for most element oxides and ±5% for Na_2O. Percent oxides were converted to Si, Ca, Mg, Na and K concentrations in mM for comparison with dissolved solutes using each oxide's gram formula weights.

Water major ion concentrations were analyzed on undiluted samples using a Dionex Model 500DX Ion Chromatograph and in-house multi-element standards. Precision was <5% based on an internal standard measured every five samples. All samples had charge balance errors <20% with 85% of the samples having <10% charge balance error; samples with large errors had low ionic strength. Si concentrations on water samples were analyzed using the Element 2 ICP. The water samples were acidified with a trace metal grade nitric acid and analyzed using a Re/Rh internal standard and a SLRS-4 reference standard.

Isotopic analyses were conducted using a Nu-Plasma multiple-collector inductively-coupled-plasma mass spectrometer (MC-ICP-MS), using the time-resolved analysis (TRA) method of Kamenov et al. (2007). For the Sr isotope analyses, on-peak zero were determined before each sample introduction in order to correct for isobaric interferences caused by impurities of Kr in the Ar carrier gas. $^{87}Sr/^{86}Sr$ was corrected for mass-bias using exponential law and $^{86}Sr/^{88}Sr=0.1194$. ^{87}Sr was corrected for presence of Rb by monitoring the intensity of ^{85}Rb and subtracting the intensity of ^{87}Rb from the intensity of ^{87}Sr, using $^{87}Rb/^{85}Rb=0.386$ and mass-bias correction factor determined from $^{86}Sr/^{88}Sr$. Average value of the TRA-measured $^{87}Sr/^{86}Sr$ of NBS 987 is 0.71024 (2σ = 0.000030). Pb analyses of NBS 981 conducted in wet plasma mode together with the sample analyses gave the following results: $^{206}Pb/^{204}Pb=16.937$ (+/-0.004 2σ), $^{207}Pb/^{204}Pb=15.490$ (+/-0.003 2σ), and $^{208}Pb/^{204}Pb=36.695$ (+/-0.009 2σ). All analyses were done at the University of Florida.

Results

Bedrock composition in the southern region is highly variable and ranges from granites to nepheline syenites, while the western region bedrock samples range from syenitic to gabbroic rocks (Fig. 4A). Bedload for the southern region is mainly syenitic in composition, varying from nepheline syenites to syeno-granites, while the bedload for the western region plots as diorites, quartz diorites, and granites (Fig. 4B). These differences are also apparent in Fig. 5, which shows the major element proportions of western and southern bedload and bedrock plotted in a ternary

diagram with Ca, Mg, and Na+K proportions as apices. This figure illustrates that the bedload compositions for both regions fall between the bedrock compositions of the region. Bedrock and bedload from the southern region plot very close to the Na+K apex with QK samples plotting the closest to the Mg apex out of all the southern watersheds (Fig. 6A). ARB and FV/RT bedrock and bedload plot closest to the Na+K apex.

Table 1. Bedload whole-rock chemistry (relative percent)

Sample Name	SiO_2	TiO_2	Al_2O_3	Fe_2O_3	MnO	MgO	CaO	Na_2O	K_2O
NA-ARB-N-2	61.03	0.20	19.43	4.29	0.17	0.21	0.49	6.99	6.42
NA-ARB-S-2	61.51	1.47	15.58	8.36	0.12	1.92	3.46	4.56	3.57
NA-ARB-S-1	63.21	0.92	15.80	6.20	0.13	1.78	3.00	5.00	4.16
NA-ARB-Mix	60.76	1.11	14.87	10.42	0.21	1.10	2.49	5.15	3.83
NA-FV-1	67.60	0.54	15.74	3.71	0.08	0.94	1.87	4.76	4.55
NA-FV-2	66.60	0.71	15.17	4.43	0.07	1.46	3.02	4.48	4.21
NA-RT-Lake	66.68	0.56	16.63	3.92	0.06	1.09	2.04	4.92	4.36
NA-RT-1	65.00	1.05	14.85	7.38	0.07	1.36	2.80	4.53	3.53
NA-RT-2	66.47	0.64	16.47	3.95	0.06	1.32	2.85	5.08	3.85
NA-RT-2 Aeolian	65.88	0.68	15.51	4.20	0.07	1.52	3.00	4.67	4.43
NA-QK-1	62.52	0.76	16.44	5.66	0.09	2.46	3.96	4.66	3.82
NA-QK-4	62.49	0.59	17.68	5.30	0.11	2.16	3.78	4.72	3.75
NA-QK-GS	63.61	0.91	15.86	6.39	0.08	2.09	3.39	4.27	3.72
NA-QK-5	58.73	1.33	15.65	9.08	0.12	3.51	4.56	4.53	3.61
KS1 Coarse	63.36	0.97	15.01	6.31	0.07	1.54	3.36	4.52	3.83
KS1 Fine	64.81	0.93	14.84	5.85	0.08	1.46	3.37	4.43	3.98
KS1 Fine Tidal	56.61	0.85	14.18	16.73	0.13	1.63	2.74	4.03	3.55
KS3	62.42	1.38	15.93	7.14	0.09	1.82	3.21	4.81	3.80
KS4	63.02	0.85	16.98	5.21	0.09	1.82	3.44	4.90	4.00

Table 2. Bedrock whole-rock chemistry (relative percent)

Sample Name	SiO_2	TiO_2	Al_2O_3	Fe_2O_3	MnO	MgO	CaO	Na_2O	K_2O
NA-ARB-N-2	69.02	0.44	15.50	2.51	0.08	0.23	0.61	5.38	6.14
NA-ARB-S-2	72.22	0.24	14.60	1.77	0.02	0.68	0.51	5.57	4.85
NA-ARB-N-1	73.29	0.13	14.41	1.47	0.03	1.42	0.18	2.85	6.22
NA-ARB-N-1	74.11	0.13	14.58	1.64	0.03	1.41	0.18	2.85	6.32
Pink cornflake	60.27	0.22	21.05	5.40	0.20	0.10	0.00	5.99	6.64
White cornflake	59.57	0.22	18.88	6.99	0.29	0.24	1.13	6.48	5.59
NA-RT-Lake	66.58	0.43	17.40	3.33	0.06	1.01	2.44	5.15	4.09
NA-RT-2	69.52	0.22	16.33	2.92	0.10	0.60	0.71	4.85	4.89
NA-RT-2 dike	58.58	1.04	14.8	11.45	0.23	0.60	2.91	5.68	5.16
FV road syenite	71.40	0.24	13.34	2.46	0.04	0.10	3.33	7.32	0.93
NA-FA-7	66.18	0.48	17.48	3.58	0.07	0.99	2.51	5.70	3.30
NA Sample near bench	62.65	0.46	18.66	3.44	0.07	0.95	3.01	7.57	2.86

Bench site near NARS	57.14	0.36	21.31	6.05	0.19	0.4	0.75	4.15	9.37
NARS bench	62.68	0.48	18.78	3.31	0.05	0.86	2.95	7.57	2.89
NA-QK-1-A	61.37	0.63	16.21	4.70	0.08	3.33	2.86	6.03	4.13
NA-QK-1-B	57.11	0.77	15.61	7.78	0.1	5.69	5.09	4.30	4.16
Outcrop below north slope between QK-2 and QK-3	75.15	0.17	13.33	1.55	0.01	0.17	0.50	4.62	5.07
NA-QK-GS	68.98	0.30	16.26	2.73	0.05	0.68	2.70	5.00	3.48
KS1 sandstone	59.75	0.38	14.09	3.64	0.10	6.98	8.46	2.87	4.26
KS1 boulder	64.99	0.43	16.24	3.73	0.07	1.35	2.62	3.92	4.86
NARS harbor	47.74	1.86	17.46	14.83	0.18	6.90	8.83	2.67	0.84

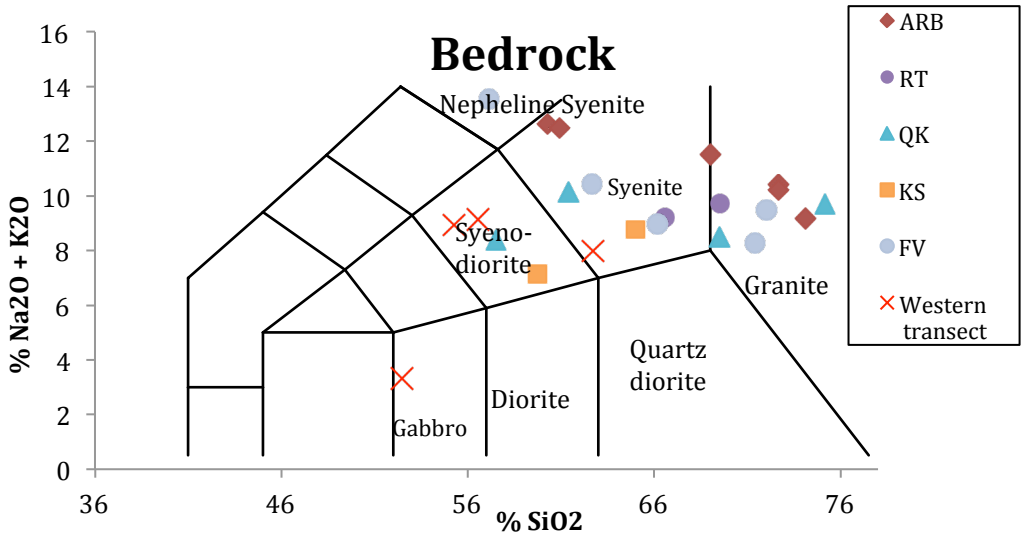

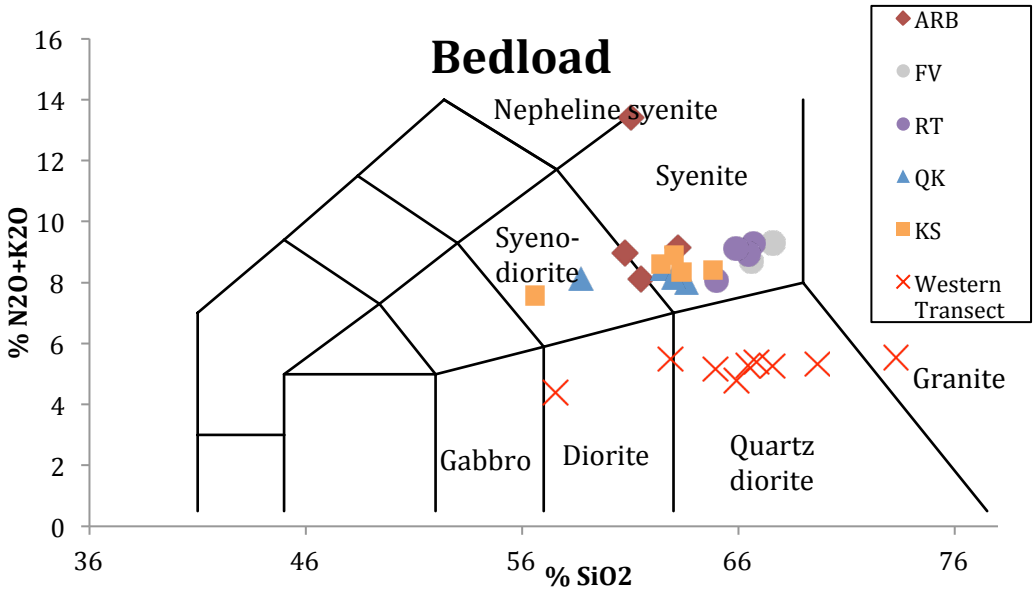

Figure 4. Total alkali-silica diagram used to identify A) bedrock compositions and B) bedload compositions, in southern and western study areas.

The major element chemistry of waters in the southern region has smaller proportions of Na+K and higher ratios of Ca/Mg compared to the bedload and bedrock (Fig. 6A). The western transect waters also have a smaller proportion of Na+K compared to the bedload and bedrock, but in these samples the relative proportions of Ca to Mg are largely unchanged (Fig 6B). As a result, all of the waters in the southern region are dominated by Ca.

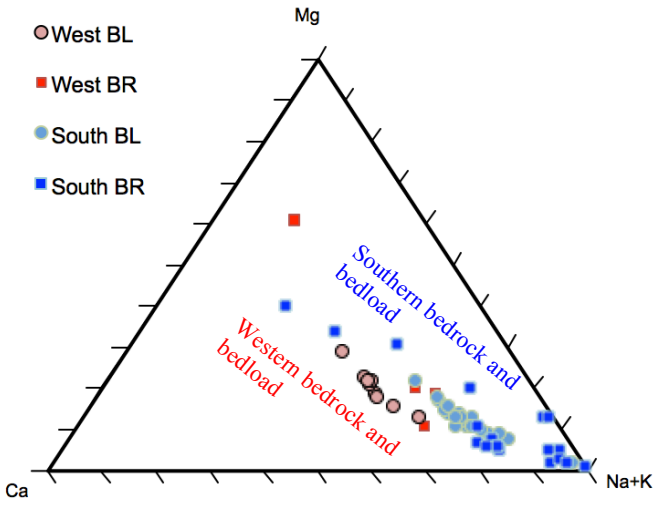

Figure 5. Ternary diagram of proportions of aerosol-corrected Ca, Mg and Na+K for southern (blues) and western (reds) bedload (BL) and bedrock (BR).

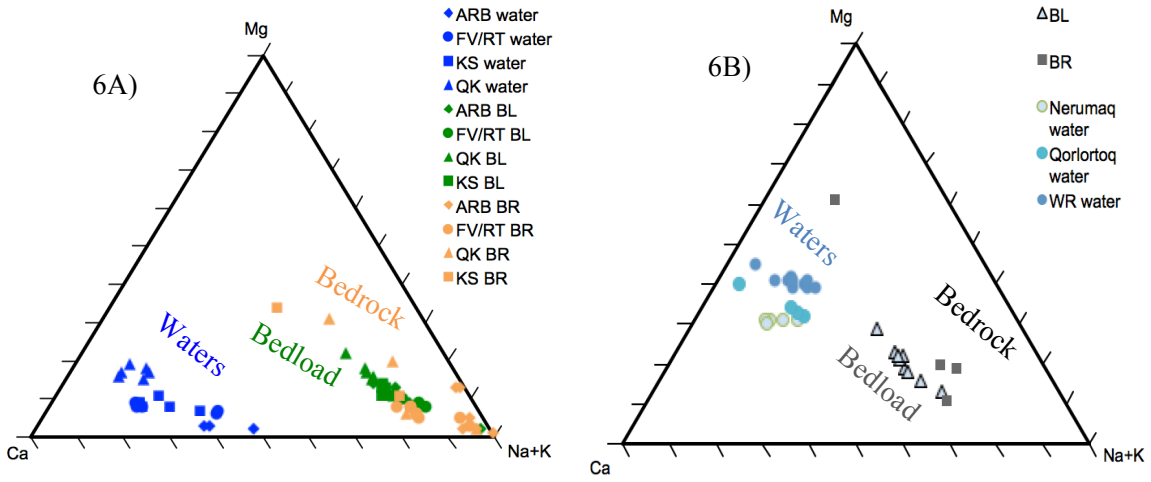

Figure 6. Ternary diagram showing the relative proportions of aerosol-corrected cations Mg, Ca and Na+K for water for A) five watersheds in the Narsarsuaq (southern) region; symbols: blue = water, green = bedload, orange = bedrock, and B) three watersheds in the western transect: symbols: circles = water, triangles = bedload, squares = bedrock.

Bedrock and bedload from QK have the highest relative proportions of Mg+Ca of all the southern sites, and ARB has the lowest proportion. Waters from QK also have the lowest

proportions of Si and Na+K, while ARB waters have the highest proportions of Si and Na+K (Fig. 7A). Bedrock, bedload, and waters from KS plot between QK, ARB, and FV/RT values.

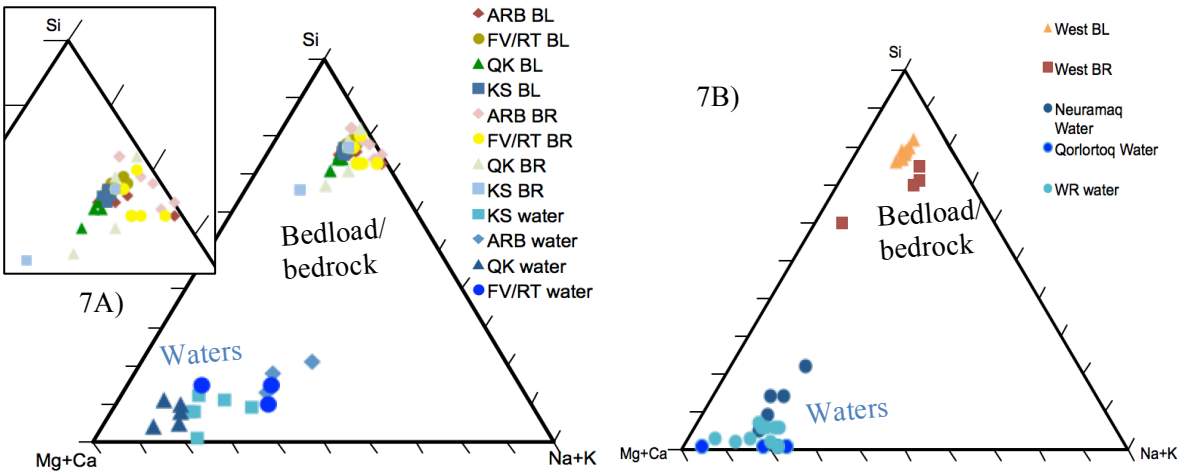

Figure 7. Ternary diagram showing the relative proportions of aerosol-corrected cations Mg+Ca, Na+K, and Si for: A) the southern region. Symbols: water (blue), bedload (darker colors), and bedrock (lighter colors). Figure on left is expanded view of the Si apex. B) The western transect. Symbols: water (blue), bedload (orange), and bedrock (red)

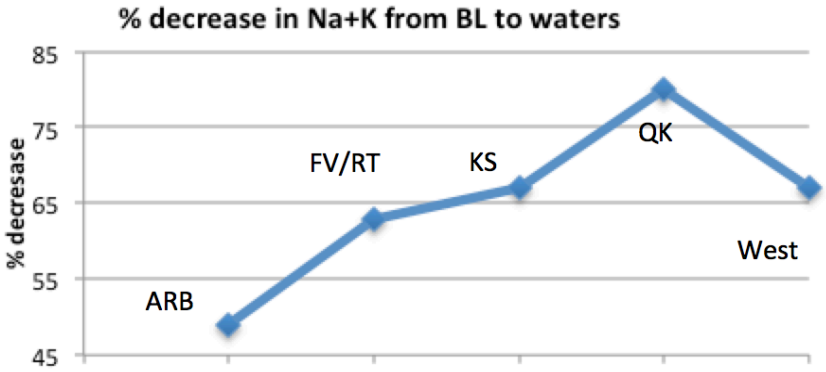

Figure 8. Average percent difference in Na+K between bedload and water for different watersheds. A smaller percent difference reflects greater weathering of silicates in the stream water.

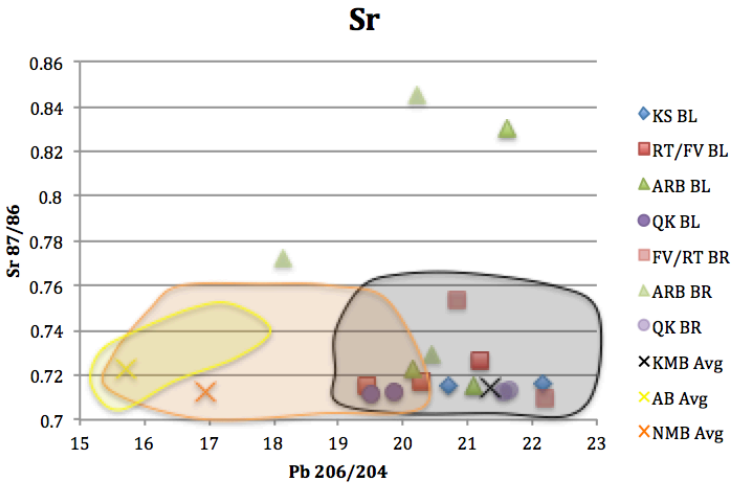

Figure 9. Isotopic data for bedrock and bedload samples in Narsarsuaq, Greenland. The X's represent the average isotopic value for the different Greenland bedrock terrains and the shaded area is the range of values for each terrain, from Reyes et al., 2014.

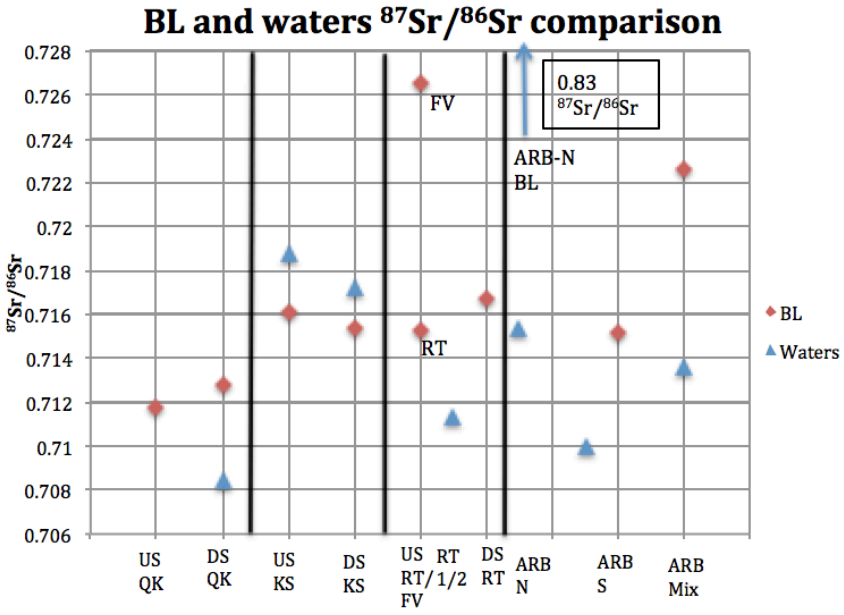

Figure 10. $^{87}Sr/^{86}Sr$ comparison between water and bedload for various watersheds in the study region. Triangles represent waters and diamonds represent BL. US = upstream and DS = downstream. Offset between samples from same watershed due to sample being taken from a slightly different area than the water sample.

$^{87}Sr/^{86}Sr$ isotope ratios (Fig. 9) are mostly concentrated between 0.7 and 0.74 and $^{206/204}Pb$ values are, for the most part, between 19-23. The sample labeled "White cornflake" and ARB-N-2 BR & BL plot anomalously high for $^{87}Sr/^{86}Sr$, and white cornflake (BR) is the only sample with a $^{206/204}Pb$ ratio of below 19. Fig. 10 illustrates that the bedload $^{87}Sr/^{86}Sr$ is more radiogenic than the waters in QK, RT/FV, and ARB. The only watershed with waters more radiogenic than the corresponding bedload is KS.

Discussion

Weathering catalysts

There are a variety of factors that play a role in chemical weathering, and the extent that each impacts weathering is unique to the area being studied. Lithology, exposure age, precipitation, climate, and vegetation all affect chemical weathering rates to some extent (Scribner et al., 2015). Bedrock is important to take into account, as it is the source of cations that are weathered into rivers, and some lithologies weather more readily than others. Depending on the rock being weathered and the acid catalyzing the weathering, the chemical reactions that occur release different solutes from the rock and have different impacts on atmospheric CO_2. This study focuses on Si, Mg, Ca, Na, and K since they are the cations released by the weathering of silicate and carbonate minerals, and thus serve as proxies for the extent of weathering. The reactions below illustrate the CO_2 uptake and weathering solutes produced by typical silicate (R1) and carbonate (R2) reactions:

$$\text{R1: } (Na,K)AlSi_3O_8 + CO_2 + 5.5H_2O \leftrightarrow (Na^+,K^+) + HCO_3^- + 0.5Al_2Si_2O_5(OH)_4 + 2H_4SiO_4$$

$$\text{R2: } CaCO_3 + CO_2 + H_2O \leftrightarrow Ca^{2+} + 2(HCO_3^-)$$

Chemical weathering preferentially attacks the minerals that are more susceptible to dissolution; therefore minerals with weaker bonds, such as carbonate minerals, will weather out faster than minerals with stronger bonds, such as silicate minerals. As a result, weathering solutes will change from those dominated by carbonate sources to those dominated by silicate sources the longer the sediments and rocks are exposed to weathering.

Although bedrock lithology impacts overall weatherability, a number of climatic factors are also important. Precipitation is included in this study because water acts as a reactant in chemical weathering, while temperature impacts the rate at which chemical reactions take place; a warmer climate is more conducive to chemical weathering than a more temperate climate under the same conditions. Vegetation, also governed by climate and precipitation, breaks down sediments into soil, that have smaller particle sizes and more organic matter that drive weathering. Plant respiration also produces CO_2, some of which is released into the soil and drives chemical weathering.

Lithologic differences between southern and western regions

Lithological differences between the southern region and western transect are apparent, this is consistent with the fact that the southern region and western transect lie within distinct geologic provinces (KMB and NMB, respectively). Rocks in the western transect range from gabbros to syenites, which tend to weather more readily than the granites in the southern region (Fig. 4A). Due to the difficulty of obtaining representative bedrock samples for each watershed, bedload data were used to develop a better understanding of the integrated composition of local bedrock sources exposed to weathering; however, the specific bedrock compositions provide more information about the endmember compositions in the watershed. Based on major cation proportions, bedload compositions in both regions plot between the compositions of local bedrock samples (Fig. 5) and integrate local bedrock sources. A crossplot of $^{87}Sr/^{86}Sr$ and $^{206/204}Pb$ ratios (Fig. 9) demonstrates that most of the bedload samples fall in the field of KMB isotopic composition (Reyes et al., 2014). Thus, the isotope chemistry suggests the bedload and bedrock are from the KMB lithological terrain. In general, bedload from the western and southern regions have similar ranges of relative percent silica and bedrock from the western region has less relative

percent Si than the southern bedrock (Fig. 7), but the southern bedrock and bedload tends to have higher relative proportions of Na+K and lower Ca/Mg than western samples (Fig. 5).

Evidence of chemical weathering extent between southern and western regions

Within the western region, the relative proportions of dissolved Ca to Mg in the water are approximately the same as the bedload and bedrock (Fig. 6B). However, in the southern region all of the water samples are enriched in Ca relative to bedload/bedrock samples from the same location, suggesting preferential weathering of trace calcite. This indicates less extensive/less mature weathering in the southern region, while the water chemistry in the western transect suggests most of the easily weatherable carbonate has been weathered out and chemical weathering is now attacking bulk rock silicates.

More extensive weathering in the western region should produce additional dissolved solutes indicative of silicate weathering. The bedload for the southern and western regions generally have similar ranges of %Si, yet the %Si in the western samples peaks at 30%, which is slightly higher than the maximum of 25% in the southern samples (Fig. 7), Thus, the Si data also support more extensive weathering in the western region.

Fig. 8 illustrates the percent change of Na+K between the bedload to the waters. A smaller percent change indicates a more similar percent composition of Na+K between bedload and its corresponding water sample. In other words, the water chemistry looks more like the bulk rock chemistry, suggesting chemical weathering of the major rock-forming silicate minerals. The western region had an average percent change of Na+K from bedload to the waters of 62%; the southern region's average was 64.75%, suggesting that on average there is more mature weathering in the western region than the southern region. In addition, percent decrease in most of the southern watersheds indicates less mature weathering than the western average. Fig. 10 shows that, on average, the waters in the southern watersheds contain less $^{87}Sr/^{86}Sr$ than the corresponding bedload. This is very different from the western transect data from Scribner et al., (2015), which reports the western transect waters are more radiogenic than the corresponding bedload. This suggests that the radiogenic phases are not weathering in the southern region, but they are being weathered in the western transect.

Weathering extent within the southern region

Within the southern region, there is a wider suite of rock types that range from silica-undersatured nepheline syenites (more weatherable) to silica-saturated granites (less weatherable) (Fig. 4A). The greatest lithologic variability occurs in FV and ARB, while QK and RT rocks generally have less weatherable lithologies. The FV/RT bedload is the most silica-rich, and ARB is the most silica-poor (Fig. 4B), since the bedrock from both watersheds plot in the same range of $\%SiO_2$, less silica in ARB bedload suggests silica has been stripped out by weathering, which is supported by the highest %Si in the waters in ARB (Fig. 7). QK and KS bedload samples plot in between these watersheds. The QK waters have the most Mg relative to Na+K and Ca out of all the southern watersheds. ARB and FV/RT waters have the most Na+K relative to Ca and Mg out of all the southern watersheds. KS waters seem to plot between these two end members. This suggests less mature weathering of carbonates that are releasing Mg into the QK waters and more mature weathering of silicate minerals in ARB and FV/RT. Fig. 7A illustrates that ARB has the most %Si in the waters in all the southern watersheds, even though it has some of the lowest %Si in the bedload; QK has some of the lowest %Si in the waters, despite the fact that the %Si of the QK bedload is similar to the other watersheds. This suggests that ARB is undergoing the most

extensive weathering in the southern region, and QK is undergoing the least extensive weathering in the southern region. This also suggests that KS is being weathered to an extent similar of the deglacial watersheds, and FV/RT is very variable. Fig. 8 also suggests that ARB is undergoing the most mature weathering, and QK is undergoing the least. Fig. 9 illustrates that the "white cornflake" sample and ARB-N-2 BL & BR have very high $^{87}Sr/^{86}Sr$ values, suggesting chemical weathering has not leached out the radiogenic phase yet. It is likely the high $^{87}Sr/^{86}Sr$ in the bedload could be the result of high initial K. Fig. 10 illustrates the isotopic differences between several water samples and the corresponding bedload samples. The QK, RT/FV and ARB waters are not as radiogenic as the bedload, suggesting the radiogenic Sr is locked in a mineral phase that is not readily susceptible to weathering. This suggests that Sr from potassium feldspar is more dominant in this system than Sr from biotite, which tends to weather out rapidly, producing waters with radiogenic $^{87}Sr/^{86}Sr$. The waters from KS have the highest $^{87}Sr/^{86}Sr$. KS is also the only watershed with waters that contain more $^{87}Sr/^{86}Sr$ than its corresponding bedload. This suggests the chemical weathering underneath the ice sheet is attacking the radiogenic phases, as opposed to the other watersheds in the south. The southern watersheds can thus be ranked in order from most weathered to least weathered: ARB, FV/RT, KS, and QK.

Implications of weathering trends

More weathering in the western region suggests that lithology is an important driver for weathering, since the lithology in this region tends to be more easily weathered. More extensive weathering in the western watersheds occurs despite lower precipitation and cooler temperatures, suggesting that, surprisingly, climate conditions in the south are not leading to greater chemical weathering. The southern region is also more vegetated, which suggests that vegetation is also not a big driver of weathering. Within the south, ARB demonstrates the highest extent of weathering as well as the most variable lithology. This relationship supports the idea that lithology can be a major driver for weathering. Vegetation and climate within the south is uniform, but exposure ages are not. QK is the oldest exposed watershed, yet QK waters have some of the lowest %Si and highest relative proportion of Ca, suggesting it is still undergoing early stages of weathering. The lithology of QK is mainly granites, which are harder to weather relative to the syenites; again supporting the idea that lithology is an important driver for weathering.

Conclusions

Based on the proportions of major cations, the chemistry of the waters in western watersheds is more similar in terms of Ca, Si, and Na+K to the bedload and bedrock than the waters in the southern region, suggesting more extensive weathering in western watersheds. The smaller percent difference between the Na+K in the southern bedload compared to bedload in the western sites indicates more mature weathering of Na- and K-rich silicates in the western region as well. Within the southern region, dissolved Si concentrations and percent differences of Na+K between the bedload and the waters suggests that ARB is the most weathered watershed, and QK is the least. This suggests that lithology is the most important control on weathering in this study. Lithology controls the mineralogy and thus the phases that will incorporate the radiogenic elements. If the radiogenic Sr is incorporated into a mineral resistant to chemical weathering, then chemical weathering will attack other minerals first. Climate, vegetation, and exposure age do not appear to control chemical weathering as much as lithology does. Recent results suggest a factor in weathering that is not accounted for in this study. Dissolved organic matter is higher in the western region; this material and subsequent microbial activity could potentially be a large driver of weathering, so further analysis of the biogeochemistry of these two study areas is needed to understand the complete picture of weathering.

ACKNOWLEDGMENTS

We'd like to thank Jon Martin for helpful discussions; the Greenland field party, Jon Martin, Shaily Rahman, and Andrea Pain, who helped with sample collection; Andrea Pain for providing the solute chemistry for the waters; Ann Heatherington for assistance with XRF; and George Kamenov for assistance with isotopic analyses. This project was funded by NSF grant OPP-1603452 and the University Scholars Program at UF. Samples were collected under Bureau of Minerals and Petroleum, Government of Greenland, Export license 027/2013.

REFERENCES

Anderson, S.P., 2007, Biogeochemistry of Glacial Landscape Systems, Annual Review of Earth and Planetary Sciences, 35:1, 375-399.

Anderson, S.P., Drever J. I., Frost C. D., and Holden P., 2000, Chemical weathering in the foreland of a retreating glacier. Geochim. Cosmochim. Acta 64, 1173–1189.

Bhatia M.P., Kujawinski E.B., Das S.B., Breier C.F., Henderson P.B. and Charette M.A., 2013, Greenland meltwater as a significant and potentially bioavailable source of iron to the ocean. Nat. Geosci. 6, 274–278.

Blum, J.D. and Erel, Y., 2003, Radiogenic isotopes in weathering and hydrology. In Treatise on Geochemistry, Surface and groundwater, weathering and soils (eds. D. Holland and K. K.Turekian). Elsevier, pp. 366–392, vol. 5

Collazo, D.F., Martin, J.B., Deuerling, K.M., 2015, Chemical Composition and Weathering of Bedrock in the Deglaciated Portion of Western Greenland, (Undergraduate thesis): University of Florida.

Deuerling, K.M., 2016, Continental Ice Sheet Retreat, Chemical Weathering, And Solute And Isotope Fluxes: Examples From Western Greenland, (Dissertation): University of Florida

Foster, G.L. and Vance D., 2006, Negligible glacial–interglacial variation in continental chemical weathering rates, Nature 444, 918–921.

Harlavan, Y. & Erel, Y., 2002, The release of Pb and REE from granitoids by the dissolution of accessory phases, Geochimica et Cosmochimica Acta, v. 66, 837-848.

Hodell, D.A., Quinn, R.L., Brenner M., and Kamenov, G.D., (2004), Spatial variation of strontium isotopes (87Sr/86Sr) in the Maya region: a tool for tracking ancient human migration, Journal of Archaeological Science, 31, 585-601.

Kamenov, G.D., Perfit, M.R., Mueller, P.A., and Jonasson, I.R., 2007, Controls on magmatism in an island arc environment: study of lavas and sub-arc xenoliths from the Tabar-Lihir-Tanga-Feni island chain, Papua New Guinea. Contrib. Mineral. Petrol., doi: 10.1007/s00410-007-0262-0.

Paslick, C.R., Halliday, A.N., Davies, G.R., Mezger, K., Upton, B.G.J., 1993, Timing of Proterozoic magmatism in the Gardar Province, southern Greenland, GSA bulletin, 105 (2), 272-278.

Pin, C., and Bassin, C., 1992, Evaluation of a Sr-specific extraction chromatographic method for isotopic analyses in geological materials. Analytica Chimica Acta, 269, p.249-255.

Reyes, A.V., Carlson, A.E., Beard, B.L., Hatfield, R.G., Stoner, J.S., Winsor, K., Welke, B., Ullman, D.J., 2014, South Greenland ice-sheet collapse during Marine Isotope Stage 11, Nature, 510, 525-528.

Scribner, C.A., Martin, E.E., Martin, J.B., Deuerling, K.M., Collazo, D.F., Marshall, A.T. 2015, Controls on weathering in deglaciated watersheds of western Greenland, Geochimica et Cosmochimica Acta, Volume 170, 157-172.

Tranter, M., 2003, Geochemical Weathering in Glacial and Proglacial Environments, Treatise on Geochemistry, 5, 189-205.

Upton, B.G.J., Emeleus, C.H., Heaman, L.M., Goodenough, K.M., Finch, A.A., 2003, Magmatism of the mid-Proterozoic Gardar Province, South Greenland: chronology, petrogenesis and geological setting, Lithos, Volume 68, Issues 1–2, 43-65

White, L.F., Bailey, I., Foster, G.L., Allen, G., Kelley, S.P., Andrews J.T., Hogan, K., Dowdeswell, J.A., Storey, C.D., 2016, Tracking the provenance of Greenland-sourced, Holocene aged, individual sand-sized ice-rafted debris using the Pb-isotope compositions of feldspars and 40Ar/39Ar ages of hornblendes, Earth and Planetary Science Letters,Volume 433, 192-203.

Wimpenny, J., James R. H., Burton K. W., Gannoun A., Mokadem F. and GıÅLslason S. R., 2010, Glacial effects on weathering processes: new insights from the elemental and lithium isotopic composition of West Greenland rivers. Earth Planet. Sci. Lett. 290, 427–437.